Article

# Supramolecular Aggregates Constructed from Gold Nanoparticles and l-Try-CD Polypseudorotaxanes as Captors for Fullerenes

Yu Liu, Hao Wang, Yong Chen, Chen-Feng Ke, and Min Liu

*J. Am. Chem. Soc.*, **2005**, 127 (2), 657-666• DOI: 10.1021/ja046294w • Publication Date (Web): 21 December 2004



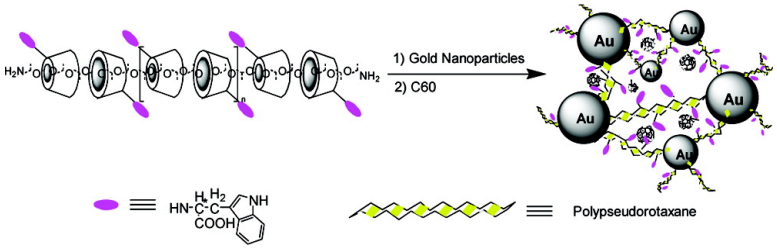


## More About This Article

Additional resources and features associated with this article are available within the HTML version:

- Supporting Information
- Links to the 9 articles that cite this article, as of the time of this article download
- Access to high resolution figures
- Links to articles and content related to this article
- Copyright permission to reproduce figures and/or text from this article

View the Full Text HTML

J|A|C|S
ARTICLES
Published on Web 12/21/2004

# Supramolecular Aggregates Constructed from Gold Nanoparticles and L-Try-CD Polypseudorotaxanes as Captors for Fullerenes

Yu Liu,* Hao Wang, Yong Chen, Chen-Feng Ke, and Min Liu

*Contribution from the Department of Chemistry, State Key Laboratory of Elemento-Organic Chemistry, Nankai University, Tianjin 300071, P. R. China*

Received June 23, 2004; E-mail: yuliu@public.tpt.tj.cn

***Abstract:*** A series of cyclodextrin-based polypseudorotaxanes (PPRs) were constructed by threading native $\beta$-cyclodextrin or L-tryptophan-modified $\beta$-cyclodextrin onto the amino-terminated PPG chains of different lengths. Subsequently, these PPRs were further assembled to form netlike supramolecular aggregates through the linkage of gold nanoparticles, and the resulting water-soluble Au−PPR aggregates were comprehensively characterized by FT-IR, UV, NMR, fluorescence spectroscopy, powder X-ray diffraction patterning, TG-DTA, and transmission electron microscopy. The results showed that the size and sedimentation rate of the Au−PPR aggregates were mainly dependent on the lengths of the PPG chains. Significantly, the Au−PPR aggregate **8**, involving many L-tryptophan residues, showed not only a satisfactory water solubility but also a good capturing ability for fullerenes in aqueous solution. The **8**−fullerene conjugate thus formed exhibited a good DNA cleavage ability under light irradiation.

## Introduction

Fullerenes have attracted a significant interest in material science owing to the combination of their unique properties, particularly their capability as electron donors or acceptors and their photophysical and photochemical behavior, that have imparted to them a number of favorable magnetic,[1] superconductivity,[2] electrical,[3] and biochemical characteristics.[4] Among the various fullerene derivatives, water-soluble fullerenes[5] have, in particular, gained popularity because of their potential biological applications.[6] In the past decade, numerous water-soluble fullerene derivatives have been synthesized, including fullerene carboxylic acid derivatives,[7] fullerene amino acid derivatives,[8] fullereneol,[9] peptide- and oligonucleotide-functionalized fullerene derivatives,[10] protein−fullerene conjugates,[11] pendant fullerene polymers,[12] main-chain fullerene polymers,[13] and dendrimeric fullerene.[14] Though these modified fullerene derivatives show moderate solubility in water, whether fullerenes really dissolve in water is still to be discovered.[4a] One possible explanation for the solubility of fullerenes in water is that they can form various supramolecular assemblies, such as vesicles, rods, capsules, and linear aggregates. Generally, two approaches have been explored to prepare such supramolecular assemblies. One approach involves covalently modifying fullerenes with

(1) (a) Makarova, T. L.; Sundqvist, B.; Hohne, R.; Esquinazi, P.; Kopelevich, Y.; Scharff, P.; Davydov, V. A.; Kashevarova, L. S.; Rakhmanina, A. V. *Nature* **2001**, *413*, 716−718. (b) Lappas, A.; Prassides, K.; Vavekis, K.; Arcon, D.; Blinc, R.; Cevc, P.; Amato, A.; Feyerherm, R.; Gygax, F. N.; Schenck, A. *Science* **1995**, *267*, 1799−1801. (c) Narymbetov, B.; Omerzu, A.; Kabanov, V. V.; Tokumoto, M.; Kobayashi, H.; Mihailovic, D. *Nature* **2000**, *407*, 883−885.
(2) (a) Schon, J.; Kloc, C.; Batlogg, B. *Science* **2001**, *293*, 2432−2434. (b) Dagotto, E. *Science* **2001**, *293*, 2410−2411. (c) Grant, P. *Nature* **2001**, *413*, 264−265.
(3) Haddon, R. C.; Perel, A. S.; Morris, R. C.; Palstra, T. T. M.; Hebard, A. F.; Fleming, R. M. *Appl. Phys. Lett.* **1995**, *67*, 121−123.
(4) (a) Nakamura, E.; Isobe, H. *Acc. Chem. Res.* **2003**, *36*, 807−815. (b) Tokuyama, H.; Yamago, S.; Nakamura, E. *J. Am. Chem. Soc.* **1993**, *115*, 7918−7919. (c) An, Y. Z.; Chen, C. H. B.; Anderson, J. L.; Sigman, D. S.; Foote, C. S.; Rubin, Y. *Tetrahedron* **1996**, *52*, 5179−5189. (d) Yamakoshi, Y. N.; Yagami, T.; Sueyoshi, S.; Miyata, N. *J. Org. Chem.* **1996**, *61*, 7236−7237.
(5) (a) Sun, Y.-P.; Lawson, G. E.; Wang, N.; Liu, B.; Moton, D. K.; Dabestani, R. In *Fullerene, Recent Advances in the Chemistry and Physics of Fullerene and Related Materials*; Kadish, K. M., Ruoff, R. S., Eds.; The Electrochemical Society Inc.: Pennington, NJ, 1997; Vol. 4, p 645. (b) Samal, S.; Choi, B. J.; Geckeler, K. E. *Chem. Commun.* **2000**, 1373−1374. (c) Brettreich, M.; Hirsch, A. *Tetrahedron Lett.* **1998**, *39*, 2731−2734. (d) Schuster, D. I.; Wilson, S. R.; Kirschner, A. N.; Schinazi, R. F.; Schlueter-Wirtz, S.; Tharnish, P.; Barnett, T.; Ermolieff, J.; Tang, J.; Brettreich, M.; Hirsch, A. *Proc. Electrochem. Soc.* **2000**, *11*, 267−270. (e) Maierhofer, A. P.; Brettreich, M.; Burghardt, S.; Vostrowsky, O.; Hirsch, A.; Langridge, S.; Bayerl, T. M. *Langmuir* **2000**, *16*, 8884−8891.
(6) Gharbi, N.; Pressac, M.; Tomberli, V.; Da Ros, T.; Brettreich, M.; Hadehouel, M.; Arbeille, B.; Trivin, F.; Céolin, R.; Hirsch, A.; Prato, M.; Szwarc, H.; Bensasson, R.; Moussa, F. In *Fullerene 2000: Functionalized Fullerene*; Maggini, M., Martin, N., Guldi, D. M., Eds.; The Electrochemical Society Inc.: Pennington, NJ, 2000; Vol. 9, pp 240−243.
(7) (a) Lamparth, I.; Hirsch, A. *Chem. Commun.* **1994**, 1727−1728. (b) Guldi, D. M.; Hungerbuhler, H.; Asmus, K. D. *J. Phys. Chem.* **1995**, *99*, 13487−13493. (c) Zhu, C.-C.; Xu, Y.; Liu, Y.-Q.; Zhu, D.-B. *J. Org. Chem.* **1997**, *62*, 1996−2000.
(8) Skiebe, A.; Hirsch, A. *Chem. Commun.* **1993**, 335−336.
(9) Chiang, L. Y.; Upasani, R. B.; Swirczewski, J. W.; Soled, S. *J. Am. Chem. Soc.* **1993**, *115*, 5453−5457.
(10) Boutorine, A. S.; Tokuyama, H.; Takasugi, M.; Isobe, H.; Nakamura, E.; Helene, C. *Angew. Chem., Int. Ed. Engl.* **1994**, *33*, 2462−2465.
(11) Sun, Y.-P.; Lawson, G. E.; Wang, N.; Liu, B.; Moton, D. K.; Dabestani, R. In *Fullerenes, Recent Advances in the Chemistry and Physics of Fullerenes and Related Materials*; Kadish, K. M., Ruoff, R. S., Eds.; The Electrochemical Society Inc.: Pennington, NJ, 1997; Vol. 4, p 645.
(12) (a) Sun, Y.-P.; Liu, B.; Moton, D. K. *Chem. Commun.* **1996**, 2699−2700. (b) Hirsch, A. *Adv. Mater.* **1993**, *5*, 859−860. (c) Geckeler, K. E. *Trends Polym. Sci.* **1994**, *2*, 355. (d) Zhang, N.; Schricker, S. R.; Wudl, F.; Prato, M.; Maggini, M.; Scorrano, G. *Chem. Mater.* **1995**, *7*, 441−442.
(13) Samal, S.; Choi, B. J.; Geckeler, K. E. *Chem. Commun.* **2000**, 1373−1374.
(14) (a) Brettreich, M.; Hirsch, A. *Tetrahedron Lett.* **1998**, *39*, 2731−2734. (b) Schuster, D. I.; Wilson, S. R.; Kirschner, A. N.; Schinazi, R. F.; Schlueter-Wirtz, S.; Tharnish, P.; Barnett, T.; Ermolieff, J.; Tang, J.; Brettreich, M.; Hirsch, A. *Proc. Electrochem. Soc.* **2000**, *11*, 267−270. (c) Maierhofer, A. P.; Brettreich, M.; Burghardt, S.; Vostrowsky, O.; Hirsch, A.; Langridge, S.; Bayerl, T. M. *Langmuir* **2000**, *16*, 8884−8891.

hydrophilic groups, especially with long chains;[15] the other involves the inclusion of unmodified fullerenes into water-soluble polymers or synthetic receptors, such as poly(*N*-vinylpyrrolidone),[16] cyclodextrins,[17] or calixarenes,[18] to form host−guest inclusion complexes or supramolecular assemblies. In the second approach, the simple incorporation of fullerenes with solubilizers might be an important but relatively less investigated method to enhance the solubility and stability of fullerenes in aqueous solution because not only can this method avoid many disadvantages of the former approach, such as the low yield and difficult separation of various isomers but also can it introduce the fullerene into a preorganized system in a more controlled fashion. On the other hand, nanometer-sized semiconductors and metal particles have also gathered increasing interest[19] in many fields, such as optoelectronics,[20] catalysis,[21] and medical diagnostics.[22] Among these particles, gold nanoparticles have attracted maximum scientific and technological attention because of their excellent physical and chemical characteristics. For example, owing to their high electron density, colloidal gold particles are commonly used as tracers in electron microscopic studies of cellular biological samples.[23] Moreover, water-soluble modified gold nanoparticles have been reported as able to act as aqueous media favorable for the manipulation of DNA and other biomolecules[24] and to enrich [60]fullerenes into nanometer-sized aggregates.[25] Recently, Mirkin et al. developed a colorimetric DNA hybridization assay using the spectral properties of gold nanoparticles.[26] In their experiments, gold nanoparticles averaging 13 nm in diameter agglutinated in the presence of DNA oligonucleotides with a matching sequence, as indicated by a color change of the sample from red to purple. Otsuka et al. reported the selective aggregation of gold nanoparticles modified by (*R*)-lactosyl-*o*-mercaptopoly(ethylene glycol) in the presence of lectin.[27] In a similar study, Hupp et al. used functionalized gold nanoparticles as spectral sensors to sense optically inert heavy metal ions via an ion-chelation-induced aggregation process.[28] More recently, we successfully constructed supramolecular assemblies bearing many metal centers through the intermolecular coordination or inclusion complexation.[29] In the current work, we wish to report a series of supramolecular networks constructed from gold nanoparticles and PPG-threaded cyclodextrin PPRs (Scheme 1). With a good preorganized structure and numerous electron donors (L-Try residues), aggregate **8**, obtained from L-tryptophan-modified $\beta$-cyclodextrin (L-Try-CD), amino-terminated PPG2000, and gold nanoparticles, was able to capture and enrich [60]fullerenes in aqueous solution through electron-transfer interactions between L-Try residues and [60]fullerenes. Interestingly, after capturing fullerenes, aggregate **8** showed an obviously enhanced DNA cleavage ability under light irradiation. These properties of aggregate **8** make it potentially applicable in the field of material technology and biological chemistry. Furthermore, it is also of our particular interest to examine factors governing the aggregation process of PPRs on nanoparticles, which will serve our further understanding of this important but minimally studied area of supramolecular chemistry.

## Experimental Section

**General.** $\alpha,\omega$-Diaminopolypropylene glycols (PPG, average molecular weight of 400, 2000, 4000) were purchased from Sigma-Aldrich. $\beta$-Cyclodextrin (CD) was purchase from Wako. L-Try-CD was prepared according to our previous report.[30] NMR spectra were recorded on a Varian INVOA 300 spectrometer in DMSO-$d_6$ using tetramethylsilane as an internal reference. FT-IR spectra were recorded on a Shimadzu Bio-Rad FTS 135 instrument. Thermogravimetric (TG) and differential thermal analyses (DTA) were obtained by using a RIGAKU standard-type spectrometer. The samples were put into platinum pans, which were hung in the heating furnace. The weight percentage of material remaining in the pan was recorded, while the temperature was increased from room temperature to 600 °C at a heating rate of 10 °C/min. Nitrogen was used as the purge gas. The X-ray diffraction scans of samples were carried out on a Rigaku D/max-2500 diffractometer. The X-ray source was Ni-filtered Cu K$\alpha$ radiation (40 kV, 100 mA). The specimens were mounted on aluminum frames and scanned from 3 to 60° $= 2\theta$ at a speed of $2\theta = 1.2°$/min. UV−vis spectra were recorded in a conventional quartz cell ($10 \times 10 \times 45$ mm) at 25 °C on a Shimadzu UV2401 spectrometer. Fluorescence spectra were measured at 25 °C using a conventional quartz cell ($10 \times 10 \times 45$ mm) on a JASCO FP-750 spectrofluorometer, with the excitation and emission slits of 5 nm width for all of the measurements, with the excitation wavelength set at 285 nm. Deionized, distilled water was used as solvent in all spectral measurements. The ICP experiment was performed on an ICP-9000 (N + M) instrument (U.S.A. Thermo Jarrell-Ash Corporation).


(15) Ros, T. D.; Spalluto, G.; Prato, M. *Croat. Chem. Acta* **2001**, *74*, 743−755.
(16) Yamakoshi, Y. N.; Yagami, T.; Fukuhara, K.; Sueyoshi, S.; Miyata, N. *Chem. Commun.* **1994**, 517−518.
(17) Diederich, F.; Gómez-López, M. *Chem. Soc. Rev.* **1999**, *28*, 263−277.
(18) Ikeda, A.; Hatano, T.; Kawaguchi, M.; Suenaga, H.; Shinkai, S. *Chem. Commun.* **1999**, 1403−1404.
(19) (a) Daniel, M. C.; Astruc, D. *Chem. Rev.* **2004**, *104*, 293−346. (b) Templeton, A. C.; Wuelfing, W. P.; Murray, R. W. *Acc. Chem. Res.* **2000**, *33*, 27−36. (c) Park, S. J.; Taton, T. A.; Mirkin, C. A. *Science* **2002**, *295*, 1503−1506. (d) Taton, T. A.; Mirkin, C. A.; Letsinger, R. L. *Science* **2000**, *289*, 1757−1760. (e) Maxwell, D. J.; Taylor, J. R.; Nie, S. M. *J. Am. Chem. Soc.* **2002**, *124*, 9606−9612.
(20) (a) Petta, J. R.; Ralph, D. C. *Phys. Rev. Lett.* **2001**, *87*, 2668011−2668014. (b) Song, Y.; Murray, R. W. *J. Am. Chem. Soc.* **2002**, *124*, 7096−7102.
(21) Guczi, L.; Petö, G.; Beck, A.; Frey, K.; Geszti, O.; Molnár, G.; Daróczi, C. *J. Am. Chem. Soc.* **2003**, *125*, 4332−4337.
(22) (a) He, L.; Musick, M. D.; Nicewarner, S. R.; Salinas, F. G.; Benkovic, S. J.; Natan, M. J.; Keating, C. D. *J. Am. Chem. Soc.* **2000**, *122*, 9071−9077. (b) Chen, S.; Ingram, R. S.; Hostetler, M. J.; Pietron, J. J.; Murray, R. W.; Schaaff, T. G.; Khoury, J. T.; Alvarez, M. M.; Whetten, R. L. *Science* **1998**, *280*, 2098−2101. (c) Niemeyer, C. M.; Bürger, W.; Peplies, J. *Angew. Chem., Int. Ed.* **1998**, *37*, 2265−2268. (d) Park, S. J.; Lazarides, A. A.; Mirkin, C. A.; Letsinger, R. L. *Angew. Chem., Int. Ed.* **2001**, *40*, 2909−2912. (e) Li, Z.; Chung, S.-W.; Nam, J.-M.; Ginger, D. S.; Mirkin, C. A. *Angew. Chem., Int. Ed.* **2003**, *42*, 2306−2309. (f) Shipway, A. N.; Katz, E.; Willner, I. *ChemPhysChem* **2000**, *1*, 18−52. (g) Perez, J. M.; Josephson, L.; Weissleder, R. *ChemBioChem* **2004**, *5*, 261−264. (h) Schellenberger, E. A.; Reynolds, F.; Weissleder, R.; Josephson, L. *ChemBioChem* **2004**, *5*, 275−279.
(23) (a) Bendayan, M. *Biotech. Histochem.* **2000**, *75*, 203−242. (b) Hainfeld, J. F.; Powell, R. D. *J. Histochem. Cytochem.* **2000**, *48*, 471−480. (c) Jurgens, L.; Nichtl, A.; Werner, U. *Cytometry* **1999**, *37*, 87−92.
(24) Niemeyer, C. M. *Angew. Chem., Int. Ed.* **2001**, *40*, 4128−4158.
(25) Liu, J.; Alvarez, J.; Ong, W.; Kaifer, A. E. *Nano Lett.* **2001**, *1*, 57−60.
(26) (a) Elghanian, R.; Storhoff, J. J.; Mucic, R. C.; Letsinger, R. L.; Mirkin, C. A. *Science* **1997**, *277*, 1078−1081. (b) Mirkin, C. A. *Inorg. Chem.* **2000**, *39*, 2258−2272. (c) Reynolds, R. A.; Mirkin, C. A.; Letsinger, R. L. *Pure Appl. Chem.* **2000**, *72*, 229−235.
(27) Otsuka, H.; Akiyama, Y.; Nagasaki, Y.; Kataoka, K. *J. Am. Chem. Soc.* **2001**, *123*, 8226−8230.
(28) Kim, Y.; Johnson, R. C.; Hupp, J. T. *Nano Lett.* **2001**, *1*, 165−167.
(29) (a) Liu, Y.; Zhao, Y.-L.; Zhang, H.-Y.; Song, H.-B. *Angew. Chem., Int. Ed.* **2003**, *42*, 3260−3263. (b) Liu, Y.; Wang, H.; Liang, P.; Zhang, H.-Y. *Angew. Chem., Int. Ed.* **2004**, *43*, 2690−2694. (c) Liu, Y.; You, C.-C.; Zhang, H.-Y.; Kang, S.-Z.; Zhu, C.-F.; Wang, C. *Nano Lett.* **2001**, *1*, 613−616. (d) Liu, Y.; Li, L.; Fan, Z.; Zhang, H.-Y.; Wu, X.; Liu, S.-X.; Guan, X.-D. *Nano Lett.* **2002**, *2*, 257−261.
(30) Liu, Y.; Han, B. H.; Sun, S. X.; Wada, T.; Inoue, Y. *J. Org. Chem.* **1999**, *64*, 1487−1493.

***Scheme 1***

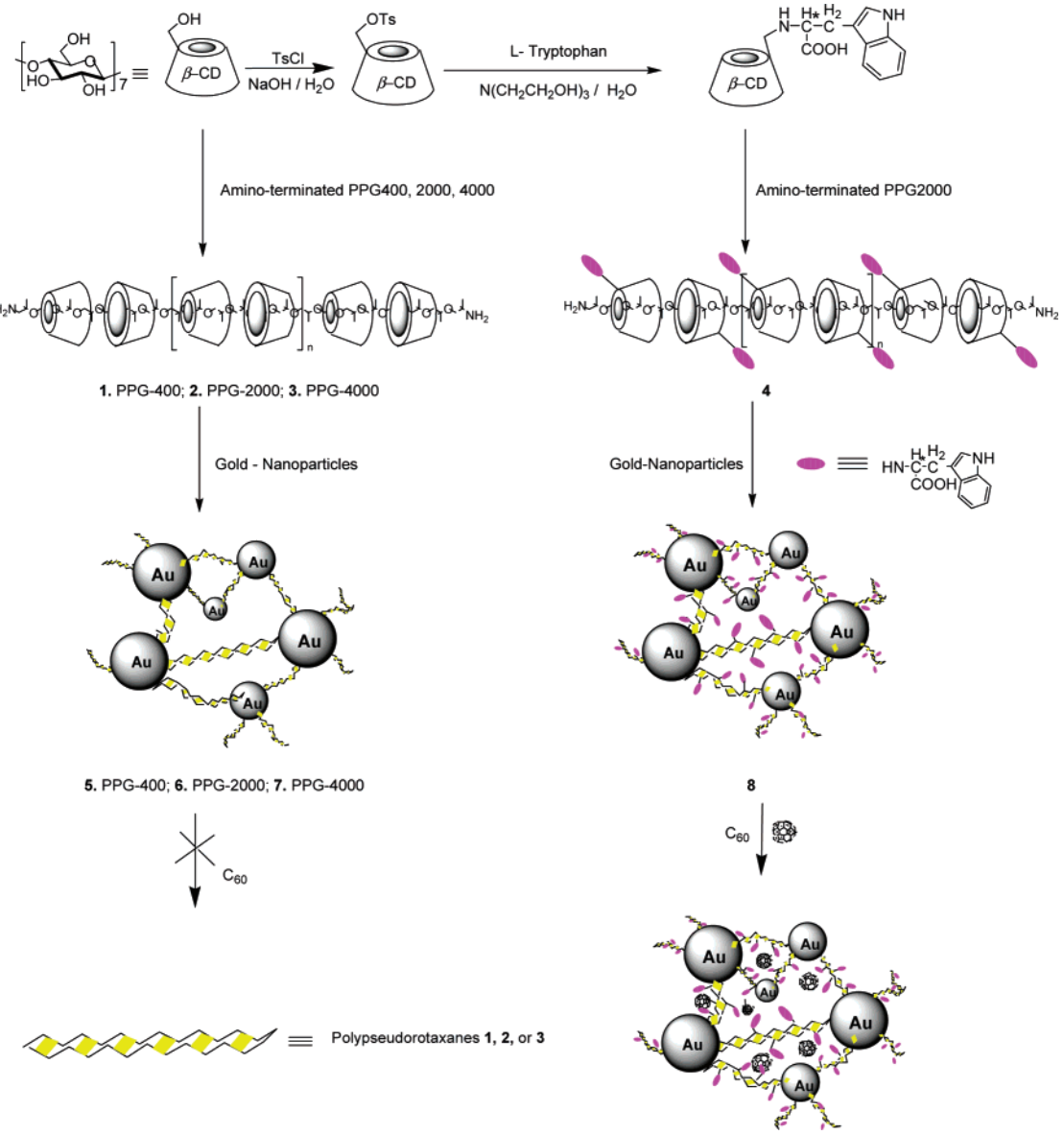


**Transmission Electron Microscopic (TEM) Measurements.** A 50 $\mu$L portion of sample solution was dropped on a copper grid. The grid was then air-dried. The samples were examined by a high-resolution transmission electron microscope (TEM) (Philips Tecnai G2 20 S-TWIN microscope) operating at an accelerating voltage of 200 keV.

**Colloid Preparation.** All glassware used in the preparation was thoroughly cleaned in aqua regia (3 parts HCl, 1 part $HNO_3$), rinsed three times with distilled water, and oven-dried prior to use. Gold colloids were prepared using a similar method reported by Frens[31] or Sutherland.[32] In a 1 L round-bottom flask equipped with a condenser, 63.7 mg of $HAuCl_4 \cdot 4H_2O$ was dissolved in 500 mL of water, and the formed 0.01% $HAuCl_4$ solution was brought to a boil with vigorous stirring. To this solution was added 7.5 mL of 1% sodium citrate. The solution turned violet-red after 1 min. Boiling was continued for an additional 10 min; then the heating source was removed, and the colloid was stirred for another 15 min. TEM data indicated an average diameter of 19.5 ± 3.4 nm. All colloids were stored at room temperature in the dark and were generally used within 1 month after preparation. Average sizes were determined by measuring diameters along a consistent axis throughout the samples.

**Synthesis of PPRs 1−3.** The PPG was mixed with a saturated aqueous solution of CD at room temperature, and the mixture was stirred overnight at room temperature. The product that precipitated was collected by filtration and washed with water and ether. Then the polypseudorotaxanes were dried in vacuo at 80 °C.

**CD−PPG400 PPR 1:** Yield 43%; IR (KBr, $cm^{-1}$) 3354, 2968, 2895, 1628, 1440, 1370, 1332, 1297, 1154, 1106, 1027, 938, 860, 756, 702, 575; $^1$H NMR (300 MHz, DMSO-$d_6$) $\delta$ 1.03−1.05 (m, 3H × 7, $CH_3$ of PPG), 3.32−3.63 (m, 42H × 3, C2-6 H of CD, 3H × 7, $-CH_2CHO-$ of PPG), 4.46−4.49 (m, 7H × 3, O-6 H of CD), 4.82−4.83 (m, 7H × 3, C-1 H of

(31) Frens, G. *Nat. Phys. Sci.* **1973**, *241*, 20−22.
(32) Sutherland, W. S.; Winefordner, J. D. *J. Colloid Interface Sci.* **1992**, *48*, 129−141.

CD), 5.70−5.77 (m, 14H × 3, O-2,3 H of CD). Anal. Calcd (%) (the number of CDs used for calculation was estimated by NMR) for $(C_{42}H_{70}O_{35})_3(C_{21}H_{42}O_7N_2H_4)(H_2O)_{22}$: C, 41.64; H, 7.13; N, 0.66. Found: C, 41.55; H, 7.44; N, 0.50.

**CD−PPG2000 PPR 2:** Yield 56%; IR (KBr, $cm^{-1}$) 3348, 2972, 2889, 1626, 1443, 1368, 1337, 1292, 1151, 1104, 1023, 942, 867, 758, 704, 565; $^1$H NMR (300 MHz, DMSO-$d_6$) $\delta$ 1.03−1.05 (m, 3H × 34, $CH_3$ of PPG), 3.27−3.66 (m, 42H × 12, C2-6 H of CD, 3H × 34, $-CH_2CHO-$ of PPG), 4.46−4.50 (m, 7H × 12, O-6 H of CD), 4.82−4.83 (m, 7H × 12, C-1 H of CD), 5.70−5.77 (m, 14H × 12, O-2,3 H of CD). Anal. Calcd (%) (the number of CDs used for calculation was estimated by NMR) for $(C_{42}H_{70}O_{35})_{12}(C_{102}H_{204}O_{34}N_2H_4)(H_2O)_{110}$: C, 41.34; H, 7.26; N, 0.16. Found: C, 41.15; H, 7.08; N, 0.25.

**CD−PPG4000 PPR 3:** Yield 26%; IR (KBr, $cm^{-1}$) 3338, 2969, 2926, 2895, 1648, 1447, 1374, 1332, 1300, 1247, 1154, 1107, 1081, 1030, 938, 860, 756, 702, 579; $^1$H NMR (300 MHz, DMSO-$d_6$) $\delta$ 1.03−1.04 (m, 3H × 68, $CH_3$ of PPG), 3.30−3.66 (m, 42H × 25, C2-6 H of CD, 3H × 68, $-CH_2CHO-$ of PPG), 4.46−4.50 (m, 7H × 25, O-6 H of CD), 4.82−4.84 (m, 7H × 25, C-1 H of CD), 5.70−5.76 (m, 14H × 25, O-2,3 H of CD). Anal. Calcd (%) (the number of CDs used for calculation was estimated by NMR) for $(C_{42}H_{70}O_{35})_{25}(C_{204}H_{408}O_{68}N_2H_4)(H_2O)_{120}$: C, 43.63; H, 7.01; N, 0.81. Found: C, 43.86; H, 6.83; N, 0.52.

**L-Try-CD−PPG2000 PPR 4:** The PPG2000 (10 mg) was put into a tube, and a saturated aqueous solution (2 mL) of L-Try-CD (64.3 mg) was added at room temperature; the mixture was ultrasonically agitated for 30 min and then allowed to stand for 48 h at 4 °C. The light-yellow precipitates were collected by centrifugation, dried under vacuum at 80 °C, washed carefully with a small amount of water and ether, and then dried under vacuum at 80 °C to give the polypseudorotaxane. Yield 6%; IR (KBr, $cm^{-1}$) 3373, 2973, 2922, 2909, 1720, 1626, 1457, 1399, 1335, 1154, 1108, 1081, 1030, 938, 860, 756, 702, 579; $^1$H NMR (300 MHz, DMSO-$d_6$) $\delta$ 1.03−1.05 (m, 3H × 34, $CH_3$ of PPG), 2.80−2.83 (m, 1 × 12, NH of Try), 3.01−3.03 (m, 3H × 12, $CH_2$ and CH of Try), 3.31−3.63 (m, 42H × 12, C2-6 H of CD, 3H × 34, $-CH_2CHO-$ of PPG), 4.47−4.56 (m, 6H × 12, O-6 H of CD), 4.79−4.83 (m, 7H × 12, C-1 H of CD), 5.69−5.80 (m, 14H × 12, O-2,3 H of CD), 6.92−6.97 (t, 1H × 12, $J$ = 6.9 Hz, aromatic H of Try), 7.02−7.06 (t, 1H × 12, $J$ = 7.5 Hz, aromatic H of Try), 7.121−7.128 (m, 1H × 12, aromatic H of Try), 7.21 (d, 1H × 12, $J$ = 2.4 Hz, aromatic H of Try), 7.54 (d, 1H × 12, $J$ = 3.9 Hz, aromatic H of Try), 10.79 (s, 1H × 12, COOH of Try). Anal. Calcd (%) (the number of CDs used for calculation was estimated by NMR) for $(C_{53}H_{80}O_{36}N_2)_{12}(C_{102}H_{204}O_{34}N_2H_4)(H_2O)_{100}$: C, 45.08; H, 7.01; N, 1.85. Found: C, 45.34; H, 6.97; N, 1.57.

**Synthesis of Au−PPR Aggregates 5−7.** To 50 mL of gold colloid solution in a round-bottom flask was added 20 equiv of saturated CD−PPG PPR solution with vigorous stirring in the dark. The pH value of the colloid solution was set at ∼6.[33] The reaction solution was maintained for 4 h, and the color of the resulting solution changed from red to violet, accompanying the appearance of precipitates. After collected by filtration, the precipitates were washed successively with water and a small amount of DMF, and then dried in vacuo to give aggregates **5**−**7** as black-blue solids.

**Aggregate 5:** Yield 34% (calculated based on the gold colloid); IR (KBr, $cm^{-1}$) 3351, 2969, 2927, 2879, 1646, 1455, 1362, 1335, 1297, 1154, 1106, 1081, 1036, 935, 861, 758, 704, 577; $^1$H NMR (300 MHz, DMSO-$d_6$) $\delta$ 1.03−1.05 (m, 3H × 7, $CH_3$ of PPG), 3.27−3.66 (m, 42H × 3, C2-6 H of CD, 3H × 7, $-CH_2CHO-$ of PPG), 4.46−4.49 (m, 7H × 3, O-6 H of CD), 4.82−4.83 (m, 7H × 3, C-1 H of CD), 5.69−5.76 (m, 14H × 3, O-2,3 H of CD).

**Aggregate 6:** Yield 47% (calculated based on the gold colloid); IR (KBr, $cm^{-1}$) 3344, 2973, 2922, 2881, 1645, 1456, 1365, 1331, 1297, 1157, 1104, 1019, 1034, 936, 863, 758, 700, 576; $^1$H NMR (300 MHz, DMSO-$d_6$) $\delta$ 1.03−1.05 (m, 3H × 34, $CH_3$ of PPG), 3.27−3.66 (m, 42H × 12, C2-6 H of CD, 3H × 34, $-CH_2CHO-$ of PPG), 4.46−4.50 (m, 7H × 12, O-6 H of CD), 4.82−4.83 (m, 7H × 12; C-1 H of CD), 5.69−5.77 (m, 14H × 12, O-2,3 H of CD).

**Aggregate 7:** Yield 52% (calculated based on the gold colloid); IR (KBr, $cm^{-1}$) 3341, 2972, 2926, 2879, 1640, 1457, 1364, 1337, 1300, 1154, 1101, 1082, 1028, 936, 857, 756, 702, 577; $^1$H NMR (300 MHz, DMSO-$d_6$) $\delta$ 1.03−1.05 (m, 3H × 68, $CH_3$ of PPG), 3.27−3.63 (m, 42H × 25, C2-6 H of CD, 3 × 68, $-CH_2CHO-$ of PPG), 4.46−4.50 (m, 7H × 25, O-6 H of CD), 4.82−4.84 (m, 7H × 25, C-1 H of CD), 5.69−5.76 (m, 14H × 25, O-2,3 H of CD).

**Synthesis of Aggregate 8.** To 10 mL of gold colloid solution in a sealed tube was added 20 equiv of saturated PPR **4** solution with vigorous stirring in the dark. The pH value of the colloid solution was set at ∼6. The reaction solution was maintained for 12 h, and the color of the resulting solution changed from red to blue-violet. The homogeneous reaction mixture was maintained at 4 °C for 3 days, and a blue precipitate was obtained. After collected by centrifugation, this precipitate was successively washed with a small amount of water and DMF and dried in vacuo to give aggregate **8** as a black-blue solid. Yield 14% (calculated based on the gold colloid); IR (KBr, $cm^{-1}$) 3371, 2973, 2921, 2908, 1716, 1626, 1454, 1396, 1333, 1158, 1105, 1082, 1030, 939, 866, 754, 703, 581; $^1$H NMR (300 MHz, DMSO-$d_6$) $\delta$ 1.03−1.05 (m, 3H × 34, $CH_3$ of PPG), 2.79−2.83 (m, 1 × 12, NH of Try), 3.01−3.03 (m, 3H × 12, $CH_2$ and CH of Try), 3.31−3.64 (m, 42H × 12, C2-6 H of CD, 3H × 34, $-CH_2CHO-$ of PPG), 4.48−4.56 (m, 6H × 12, O-6 H of CD), 4.80−4.83 (m, 7H × 12, C-1 H of CD), 5.71−5.81 (m, 14H × 12, O-2,3 H of CD), 6.92−6.96 (t, 1H × 12, $J$ = 6.0 Hz, aromatic H of Try), 7.02−7.05 (t, 1H × 12, $J$ = 4.5 Hz, aromatic H of Try), 7.122−7.128 (m, 1H × 12, aromatic H of Try), 7.21 (d, 1H × 12, $J$ = 2.4 Hz, aromatic H of Try), 7.54 (d, 1H × 12, $J$ = 3.9 Hz, aromatic H of Try), 10.81 (s, 1H × 12, COOH of Try).

**General Synthesis Procedure of Aggregate−Fullerene System.** An excess amount of [60]fullerene was added to a saturated polypseudorotaxane−Au aggregate solution (10 mL). The reaction mixture was stirred for 12 h, and the insoluble matter was removed by centrifugation (16 000 rpm). After the solvent was removed under the reduced pressure, the obtained [60]fullerenes-containing aggregate was dried in vacuo to give a brown-black solid. The UV−vis spectrum was used to monitor whether [60]fullerenes were incorporated into the aggregates

(33) Zheng, J. W.; Zhu, Z. H.; Chen, H. F.; Liu, Z. F. *Langmuir* **2000**, *16*, 4409−4412.

***Scheme 2***

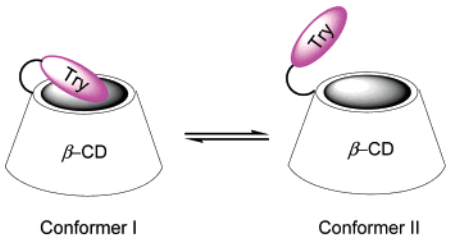


by examining the characteristic absorption maximum of [60]-fullerenes in aqueous solution.

## Results and Discussion

**Preparation and Characterization of PPRs: Preparation of PPRs.** CD-based PPRs **1**−**4** were prepared by adding the amino-terminated PPGs ($M_n$ = 400, 2000, 4000) to a saturated aqueous solution of $\beta$-CD or L-Try-CD and stirring the mixture at room temperature. During this process, the clear solution became turbid, and the PPRs were formed as crystalline precipitates. For $\beta$-CD PPRs, the threading of CD cavities onto PPG chains was rapid, with a satisfactory yield of 26−56%. Generally, the PPRs would precipitate after the reaction mixture was stirred for $^1/_2$ h. However, the yield of L-Try-CD PPR was relatively low (6%), which indicated that L-Try-CD was somewhat difficult to thread onto the PPG chains. One possible reason for this might be the conformational equilibrium between the free and self-included conformer of L-Try-CD in the aqueous solution (Scheme 2).[30]

With the addition of PPG, the free L-Try-CD (conformer II) spontaneously formed a complex with the PPG chain to give the PPR precipitate, which subsequently led to the equilibrium shift from conformer I to conformer II. Because of the strong self-inclusion ability of L-Try-CD,[30] most of the L-Try-CD molecules are expected to exist as the conformer I in the initial stage, which is unfavorable to the threading of PPG into the CD cavity. Therefore, a longer reaction time is necessary for the preparation of L-Try-CD PPR. From the $^1$H NMR data of PPRs **1**−**4** (Figure 1), we could calculate the number of CD units in **1**−**4** by comparing the integral of the signals at 4.8 ppm (C-1 H of $\beta$-CD) with those at 1.03 ppm ($CH_3$ of PPG).[34] The obtained values were 3 (for **1**), 12 (for **2**), 25 (for **3**), and 12 (for **4**), which means PPG400, 2000, and 4000 could thread 3, 12, and 25 CD cavities to form the PPRs, respectively. These results indicated that, by selecting the appropriate PPG chains, we could control the number of CD units in PPR, which would provide a versatile method for the design and preparation of CD-based pseudorotaxanes.

Besides the high solubility in DMF and DMSO, PPRs **1**−**3** also showed an appreciable water solubility at room temperature, and their water solubility decreased with the elongation of the PPG chain. It is worth noting here that the water solubility of L-Try-CD PPR **4** was obviously higher than those of CD PPRs **1**−**3**, which might be attributed to the solubilization effect of the hydrophilic L-Try residues in **4**.

**Morphology and Thermal Stability of PPRs.** Figure 2 shows the XRD patterns of PPRs **1**−**4**. As can be seen from Figure 2, the patterns of PPRs **1** and **2** are similar to that of the CD−*p*-nitroacetanilide complex, which has been proven to have a columnar structure by X-ray single-crystal studies,[35] indicating that PPRs **1** and **2** are crystalline in the solid state and possess a columnar structure. Moreover, although the relative intensities and some reflection angles of peaks in the XRD patterns of **3** are different from those of **1** and **2**, its prominent strong peaks ($2\theta$) at 11.56 and 17.94° also indicate the formation of the inclusion complexes between CD channels and PPG4000.[36] The differences of the peak patterns are likely to be attributed to the decrease of the crystalline ordered degree with the increase of the polymeric chain. However, the diffractogram of L-Try-CD PPR **4** is not consistent with those of **1**−**3**, in that the XRD pattern of **4** shows a trend of a broad diffuse halo, indicating that **4** is amorphous to some extent, which might result from the fact that the L-Try residues have more freedom and complicated spatial conformation conversion. Even so, PPR **4** still adopts the channel structure like those of **1**−**3**. A series of characteristic reflections of **4** (Figure 2d) at $2\theta$ = 7.22° ($d$ = 12.23 Å), 9.20° ($d$ = 9.60 Å), 12.20° ($d$ = 7.25 Å), 17.50° ($d$ = 5.06 Å), and 18.84° ($d$ = 4.71 Å) are quite similar to those of its analogue **2** (Figure 2b) at $2\theta$ = 7.16° ($d$ = 12.33 Å), 9.58° ($d$ = 9.22 Å), 12.52° ($d$ = 7.06 Å), 17.62° ($d$ = 5.03 Å), and 18.80° ($d$ = 4.72 Å). The thermogravimetric (TG) measurements of PPRs **1**−**4** show that they start to decompose at 280−300 °C and entirely decompose at ca. 510 °C. The differential thermal analysis results (DTA) show exothermic peaks of **1**−**4** at ca. 340 °C, referring to the decomposition of CD units in PPRs. Taking into consideration that the native $\beta$-CD decomposes below 310 °C, this phenomenon indicates that PPG plays a stabilizing role for **1**−**4**. Moreover, the weight losses under 100 °C of **1**−**4** are shown to be 8.2, 9.8, 5.6, and 9.5%, respectively, validated by TG experiments, which is consistent with the known mass fraction values of water molecules calculated by elemental analysis, which are 9.34, 11.24, 6.26, and 10.55%, respectively, for polypseudorotaxanes **1**−**4**.

**Preparation and Characterization of Au−PPR Aggregates: Preparation of Au−PPRs.** The gold colloidal dispersions were prepared through the reduction of $AuCl_4^-$ by citrate. When a saturated PPR solution is added to a gold colloid, the citrates that are absorbed around the surface of gold colloid particles are replaced by PPR through electrostatic interactions.[19a] Therefore, the surface of Au particles becomes hydrophobic, and the colloidal stability in aqueous solution is reduced. Subsequently, the resulting Au−PPR aggregates precipitate out from the aqueous environment. The aggregation process of nanoparticles can be monitored easily by examining the color change of the reaction system. Usually, when interparticle distances are substantially greater than the average particle diameter, the gold nanoparticles are red in color because of the Mie absorption by their surface plasmon oscillation that peaks at 520 nm.[37] However, with the aggregation proceeding, the color of the aggregates turns blue when the interparticle distance in these aggregates decreases to less than approximately the average particle diameter.[38] In our experiments, all of the Au−PPRs **5**−**8** display the color change from red to violet (or blue-

(34) Liu, Y.; Li, L.; Zhang, H.-Y.; Zhao, Y.-L.; Wu, X. *Macromolecules* **2002**, *35*, 9934−9938.
(35) (a) Harding, M. M.; Maclennan, J. M.; Paton, R. M. *Nature*, **1978**, *274*, 612−615. (b) Harada, A.; Okada, M.; Li, J.; Kamachi, M. *Macromolecules* **1995**, *28*, 8406−8411.
(36) Huang, L.; Tonelli, A. E. *J. Macromol. Sci., Rev. Macromol. Chem. Phys.* **1998**, *C38* (4), 781.
(37) Takeuchi, Y.; Ida, T.; Kimura, K. *Surf. Rev. Lett.* **1996**, *3*, 1205−1208.
(38) Kreibig, U.; Genzel, L. *Surf. Sci.* **1985**, *156*, 678−700.

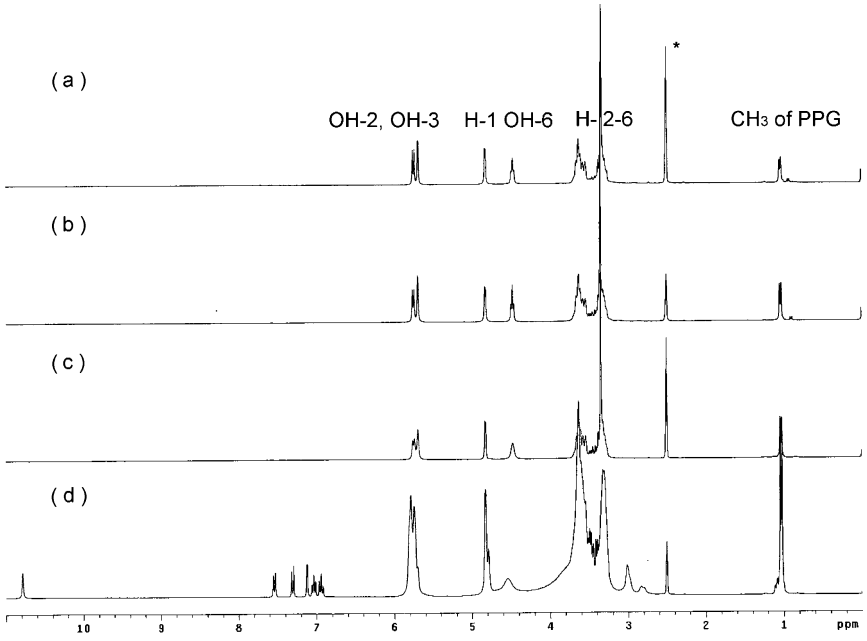


***Figure 1.*** $^1$H NMR spectra of (a) **1**, (b) **2**, (c) **3**, and (d) **4** in DMSO-$d_6$. Asterisk denotes the solvent peaks.

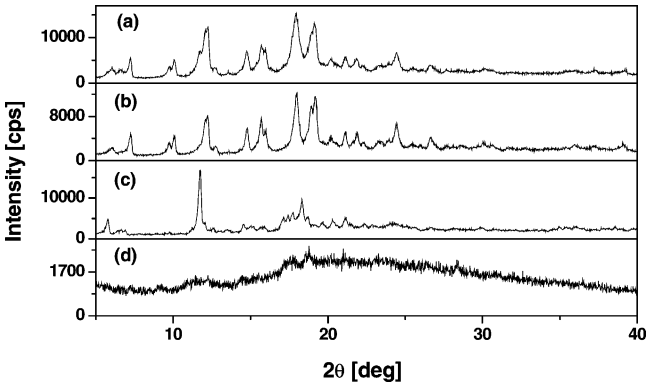


***Figure 2.*** X-ray diffraction patterns for PPR **1** (a), **2** (b), **3** (c), and **4** (d).

violet) during the reaction procedure, indicating the aggregation of Au nanoparticles. It is important to clarify that the formation of the polypseudorotaxanes **1**−**4** through the inclusion complexation of CDs and polymers is an equilibrium process. It is possible to see dethreading taking place due to the redissolution of isolated polypseudorotaxanes. Therefore, we took several methods to prevent, as much as possible, any dethreading of CDs from the polymers. First, we performed the reaction in water to maintain the hydrophobic interactions between the CD cavities and polymers. Second, in the preparation process, the PPR solution was saturated, which served to drive the equilibrium toward the formation of the inclusion complexes between CDs and PPG chains. Finally, during the purification, the crude products were washed successively with water and DMF/ether, which would remove the byproducts (CD, PPG, and PPG/Au−NP aggregates) resulting from the dethreading of PPRs because CD is soluble in water, while PPG and PPG/Au−NP aggregates are quite soluble in DMF/ether. These attempts would efficiently avoid the unfavorable influence of the dethreading. It is worth noting that the yield of aggregate **8** (14%) was lower than those of aggregates **5**−**7** (34−52%), which can possibly be attributed to the high hydrophilicity of L-Try residues in **8** making it unfavorable for its precipitation from the aqueous solution. Hence, a long time and relatively low temperature are necessary to enable complete precipitation of **8**.

**Solubility Experiments of the Aggregates.** Aqueous solubility of aggregates **5**−**7** in water at room temperature was determined gravimetrically. In a typical experiment, 100 mg of a sample was added to 5 mL of water. After the mixture was sonicated for 30 min, the aggregate−water mixture was centrifuged, followed by the removal of the clear aqueous solution. The residual aggregate sample was dried, and its weight was determined and used in the solubility calculation. The solubility of aggregate **8** was determined with the same procedure by adding 30.4 mg of aggregate **8** to 1 mL of water. The calculated solubilities of aggregates of **5**−**8** were 9.3, 4.7, 2.6, and 27.1 mg/mL, respectively. The obtained results clearly show that the solubility of aggregate **8** is higher than that of the other three aggregates.

**$^1$H NMR Spectra.** $^1$H NMR experiments showed that there were 3, 12, and 25 $\beta$-CD units threaded on average onto the PPG400, 2000, and 4000 chains, respectively. After being adsorbed on the surface of Au particles, the integral ratios between the H-1 protons of $\beta$-CD and the methyl protons of PPG chains were basically unchanged, indicating that the $\beta$-CD units were not dethreaded out of the PPG chains in the absorption process. Moreover, it is well-known that the presence of metal centers in liquid-phase NMR samples can generate large inhomogeneities in the magnetic field about the local chemical environments.[39] Therefore, when the PPRs are adsorbed on the surface of the Au particles through their thio or amino groups, the proton peaks could show the intensity, shift, or breadth changes relative to those of the native compounds.[40] In the present case, the comparison of the partial NMR spectra of PPR and Au−PPR showed that the signals at 2.87 ppm in Figure 3a, assigned to the N−$CH_2$ protons in the amino-terminated PPG chains, disappeared in the NMR spectrum of the Au−

(39) Bradley, J. S. The Chemistry of Transition Metal Colloids. In *Clusters and Colloids: From Theory to Applications*; Schmid, G., Ed.; VCH Publishers: New York, 1994; Chapter 6, p 517.
(40) Liu, J.; Alvarez, J.; Kaifer, A. E. *Adv. Mater.* **2000**, *12*, 1381−1383.

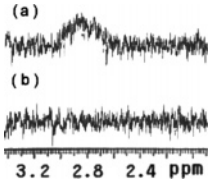


***Figure 3.*** Partial $^1$H NMR spectra of (a) PPR **1** and (b) Au−PPR aggregate **5** in DMSO-$d_6$.

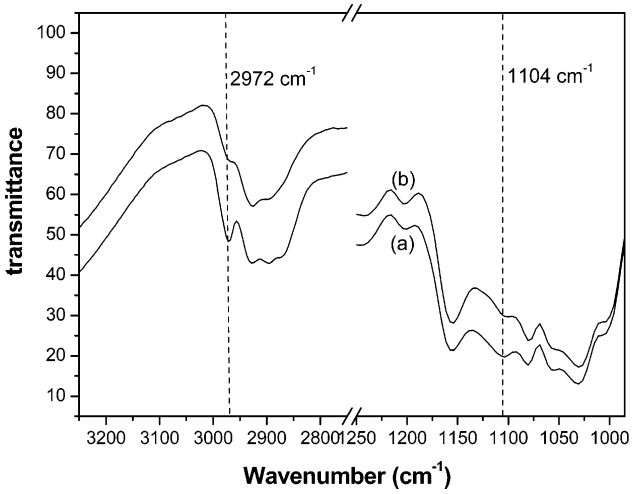


***Figure 4.*** FT-IR spectra of (a) PPR **2** and (b) Au−PPR aggregate **6**.

PPR aggregate (Figure 3b), which could possibly be attributed to the fact that this peak underwent a great shift and convoluted with other broad multiplets. Similar results were observed in the characterization of the primary amide-capped Au nanoparticles and oleylamine-capped Au nanoparticles.[41]

**FT-IR Spectra.** When the primary amines were adsorbed on the surface of the gold nanoparticles, some characteristic vibration band changes can be employed to validate whether the primary amines have been attached to the gold nanoparticles. Therefore, we performed the FT-IR spectra of Au−PPR aggregates **5**−**8** and their precursors **1**−**4**. Figure 4 illustrates the typical IR spectra of **2** and **6**, which was used as a representation of IR spectra of Au−PPR aggregates and their precursors. As can be seen in Figure 4, the IR spectrum of Au−PPR aggregate **6** is quite similar to that of its precursor (without Au−NPs) **2** with several small differences, including the following. (1) The bands of methylene stretches at 2972 cm$^{-1}$ corresponding to the hydrocarbon chains of PPG in PPRs decrease after the reaction with Au nanoparticles, indicating that these hydrocarbon chains surrounding the nanoparticles are highly ordered in the solid state.[42] (II) The intensity of the bands at 1104 cm$^{-1}$ (C−N stretch) in the IR spectra of Au−PPR aggregates becomes stronger, accompanied by an appreciable band broadening, as compared to the corresponding bands of PPRs. These two characteristic changes in the IR spectra[41] indicate that the PPRs are successfully adsorbed on the surface of the Au nanoparticles through their terminal amine groups.

**X-ray Powder Diffraction.** The crystallization of PPRs on the surface of Au nanoparticles was investigated by XRD since the XRD pattern of a sample can probe a large number of statistically oriented crystallites.[42] Figure 5 shows the typical

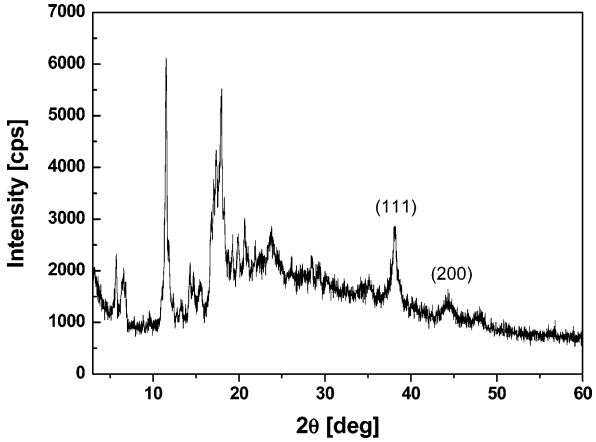


***Figure 5.*** XRD pattern of Au−PPR aggregate **7**.

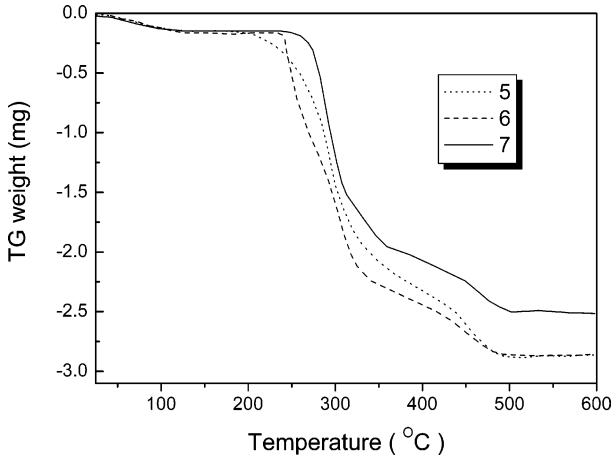


***Figure 6.*** Weight-loss curves of Au−PPR aggregates **5**−**7** under dry nitrogen purge.

XRD patterns of Au−PPR aggregate **7**. As shown in Figure 5, besides the characteristic reflection of the PPR unit, two new reflection signals appear at ca. $2\theta = 38.1$ and 44.4° in the XRD pattern of the Au−PPR aggregate **7**, corresponding to the (111) and (200) planes of the cubic phase of Au, respectively. Moreover, the average size of the gold nanoparticles was also determined from the width of the reflection according to the Scherrer formula $D = 0.9\ \lambda/(\beta \cos \theta)$, where $\beta$ is the half-maximum line width, $\theta$ the angle of reflection, and $\lambda$ the wavelength of the X-ray radiation.[43] The value of $D$ calculated from the (111) reflection of the cubic phase of Au was ca. 25 nm, which is basically in agreement with the results of transmission electron microscopy (TEM) experiments.

**Thermogravimetric Analysis.** Thermogravimetric analysis has been conveniently used before to monitor the decomposition temperature and to acquire information about the organic composition of monolayer-protected nanoparticles.[19a] Figure 6 shows the weight-loss curve of Au−PPR aggregates **5**−**7**. Generally, the decomposition onset temperature of a sample depends on how it is defined, as well as many other factors, including the purge gas, heating rate, and sample geometry (i.e., exposed surface area-to-volume ratio). For our purpose, it was defined as the temperature at which 7% weight loss was reached. Using this definition, the decomposition onset temperatures of

(41) Leff, D. V.; Brandt, L.; Heath, J. R. *Langmiur* **1996**, *12*, 4723−4730.
(42) (a) Hostetler, M. J.; Stocks, J. J.; Murray, R. W. *Langmuir* **1996**, *12*, 3604−3612. (b) Mayya, K. S.; Caruso, F. *Langmuir* **2003**, *19*, 6987−6993.
(43) Cullity, B. D. *Elements of X-ray Diffraction*, 2nd ed; Addison-Wesley: Reading, MA, 1978; p 99.

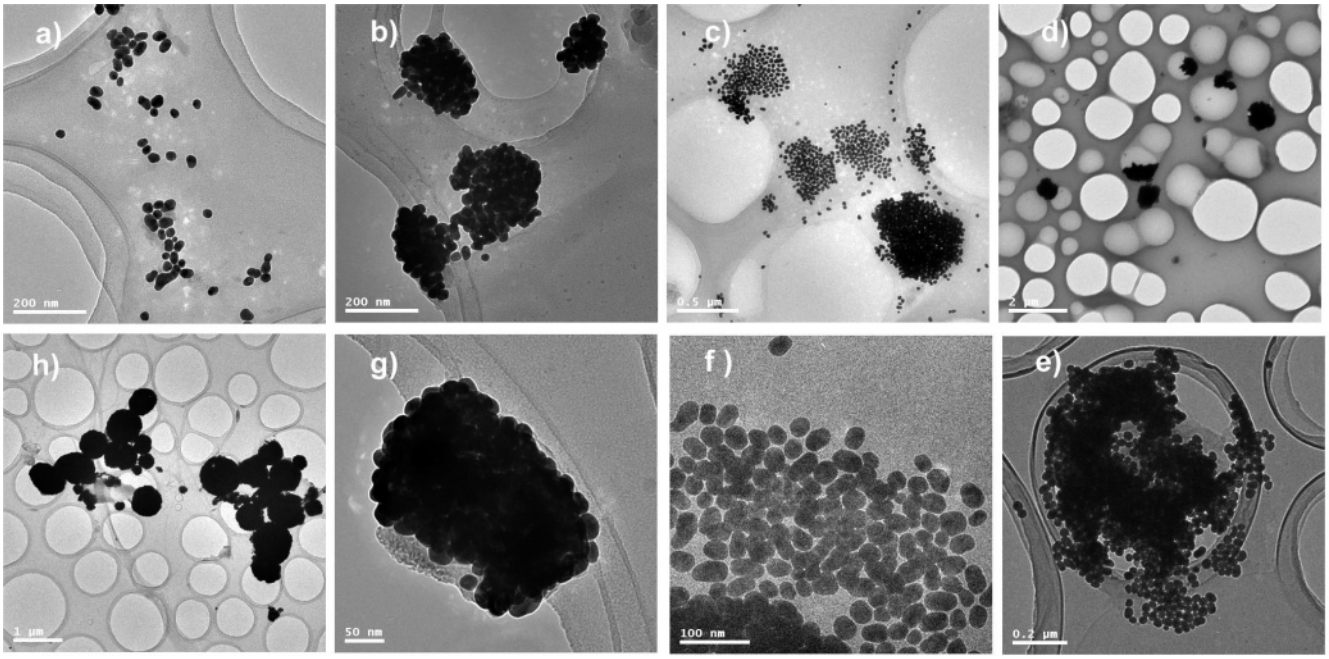


***Figure 7.*** TEM images of (a) Au colloid particles, (b) Au−PPR aggregates **5**, (c) **6**, (d) **7**; (e−g) high-resolution TEM images of (e) **5**, (f) **6**, and (g) **7**; (h) TEM image of Au−PPR aggregate **8**.

**5**−**7** were 214, 242, and 260 °C, respectively, indicating that the thermal stability of the Au−PPR aggregates increased with the elongation of the PPG chain. Furthermore, the residual contents (wt %) for aggregates **5**−**7** at a temperature over 600 °C are 0.9, 0.7, and 0.7%, respectively, which could be considered as the gold content in aggregates **5**−**7**. In addition, to corroborate these data, we also performed the ICP experiments to determine the gold content in the aggregates. The ICP results are 0.92, 0.80, and 0.74% for aggregates **5**−**7**, respectively, which are basically consistent with the data obtained from the DTA analysis. Moreover, the polypseudorotaxane contents in the Au−(PPG*n*⊂CD) (*n* represents the average molecular weight of PPG400, 2000, and 4000) are 85.8, 92.4, and 92.8% for Au−(PPG400⊂CD), Au−(PPG2000⊂CD), and Au−(PPG4000⊂CD), respectively, if we consider that the weight loss from 200 to 600 °C is attributed to the polypseudorotaxane. To simplify the calculation, the core shape of the nanoparticles is assumed to be spherical. Therefore, the polypseudorotaxane numbers on each of the nanoparticles are calculated to be 243, 73, and 40 for Au−$(PPG400⊂CD)_{0.5}$, Au−$(PPG2000⊂CD)_{0.5}$, and Au−$(PPG4000⊂CD)_{0.5}$, respectively. The average surface area occupied by one polypseudorotaxane is 20.67, 68.82, and 125.60 $nm^2$ for **5**, **6**, and **7**, respectively. Although all of these values are approximate, we still could draw a conclusion that, with the increase of the molecular weight of polypseudorotaxane, the footprint is also increased.

**Transmission Electron Microscopy (TEM).** Direct information about the shape, size, and size distribution of the aggregates came from the high-resolution transmission electron microscopy (HR-TEM) results. Figure 7a shows the HR-TEM images of Au colloids. Under our experimental conditions, the average gold core size of Au nanoparticles was 19.5 ± 3.4 nm (statistical particles were 230). When the PPRs were added to the gold colloidal solution, Au−PPR aggregates were formed with average aggregate sizes of ca. 200 nm for **5**, 400 nm for **6**, 800 nm for **7**, and 450 nm for **8**. Although the aggregate size distribution was found relatively broad and the number of the examined aggregates was limited (statistical aggregates were ca. 50−80 for each measurement), it still could be recognized that the average aggregate size tended to increase with the elongation of the PPR used. This concept will efficiently facilitate the design and synthesis of new supramolecular architectures with special size.

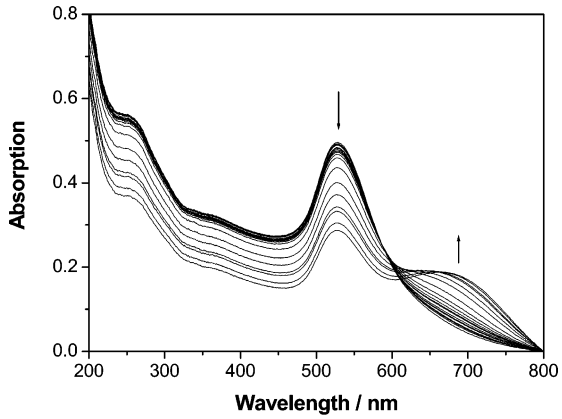


***Figure 8.*** Time-dependent UV−vis spectra of aggregate **6** (0.3 mg/mL). The curves from top to bottom correspond to the gradual increment of time: 0, 1, 2, 3, 5, 10, 15, 20, 25, 32, 45, 60, 90, 120, 150, 180, 190 min.

**Sedimentation Rates of Au−PPR Aggregates.** Measurement of the sedimentation rate has been reported to be a convenient method for evaluating the aggregation process of Au nanoparticles.[43] Herein, we employed this concept to qualitatively analyze the aggregation behavior of Au−PPRs. Sedimentation rates of the Au−PPR aggregates **5**−**7** were monitored by following the intensity of the surface plasmon (SPR) band maximum at 528 nm as a function versus time. As can be seen in Figure 8, the SPR band of Au particles at 528 nm gradually decreases, while a new SPR band appears at 665 nm and gradually increases. This phenomenon might indicate the formation of the Au−PPR aggregates since the aggregation of gold nanoparticles usually leads to the appearance of a new absorption band at a wavelength longer than that of the discrete

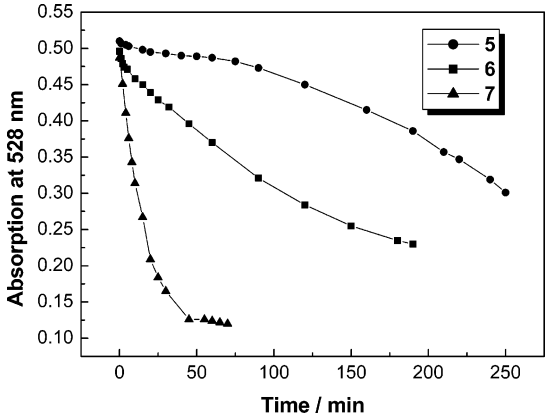


***Figure 9.*** Sedimentation rates of aggregates **5**−**7** denoted by the SPR intensities of aggregates **5** (0.1 mg/mL), **6** (0.3 mg/mL), and **7** (0.6 mg/mL).

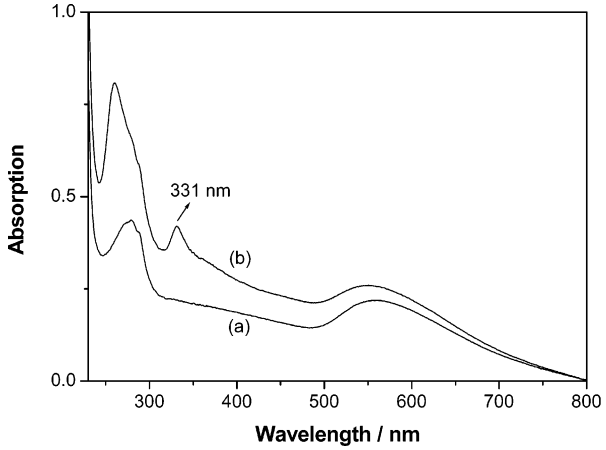


***Figure 10.*** UV−vis spectra of (a) aggregate **8** (0.2 mg/mL) and (b) [60]-fullerene-absorbed aggregate **8** in aqueous solution.

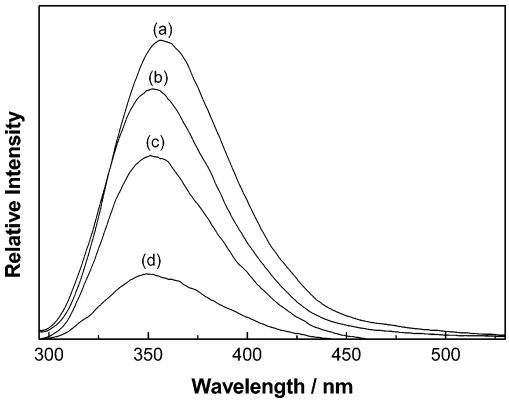


***Figure 11.*** Fluorescence spectra of (a) L-Try-CD ($5.0 \times 10^{-6}$ M), (b) L-Try-CD ($5.0 \times 10^{-6}$ M) + PPG2000 ($5.0 \times 10^{-7}$ M), (c) L-Try-CD ($5.0 \times 10^{-6}$ M) + PPG2000 ($5.0 \times 10^{-7}$ M) + Au colloid ($5.0 \times 10^{-8}$ M), and (d) L-Try-CD ($5.0 \times 10^{-6}$ M) + PPG2000 ($5.0 \times 10^{-7}$ M) + Au colloid ($5.0 \times 10^{-8}$ M) + $C_{60}$.

Au nanoparticles as a result of the electric dipole−dipole interactions and the coupling between the plasmons of neighboring particles in the formed aggregates.[44] On the other hand, from the absorption/time plot shown in Figure 9, we can seen that aggregates **5**−**7**, constructed from Au nanoparticles and PPRs of different lengths, displayed significantly different sedimentation rates during aggregate formation, especially in the initial stages. Thus, aggregate **5**, possessing the shortest PPR linkers, exhibited a mild decrease of the SPR maximum. However, the SPR maximum of aggregate **7**, constructed from the longest PPR linkers, showed a rapid decline against time, and 75% of the SPR absorption of **7** was quenched within 45 min. Furthermore, aggregate **6** displayed a behavior between these two extremes and gave a moderate sedimentation rate.

**Captor for [60]Fullerene**. While performing our experiments, we observed that aggregate **8**, different from other aggregates, showed a higher water solubility and a better preorganized structure, as seen in pseudopeptides. Inspired by some other reports about the interactions of [60]fullerenes or its derivatives with biological cells,[45] we hypothesized that the aggregates might possess the capability of capturing and enriching [60]fullerenes in the aqueous solution. This hypothesis was further validated by the following experiments. Solid [60]-fullerene (20.3 mg) was added to a saturated aggregate **8** solution (10 mL). After the reaction mixture was stirred for 12 h, the insoluble matter was removed by centrifugation (16 000 rpm). The solvent was then removed under reduced pressure conditions, and the obtained [60]fullerenes-adsorbed aggregates were dried in vacuo to give a brown-black solid. The appearance of an absorption maximum at 331 nm in the UV−vis spectrum of the **8**−[60]fullerene system (Figure 10), as well as a typical FT-IR band at 527 $cm^{-1}$ assigned to the [60]fullerene unit in **8**, indicated the effective enrichment of **8** toward [60]fullerene. The enrichment ability of aggregate **8** toward [60]fullerene in aqueous solution was quantitatively evaluated by solubility experiments using a method previously reported.[31,46] Aggregate **8** (2.3 mg) was dissolved in 1 mL of water, and then 5.0 mg of solid [60]fullerene was added to the resultant solution. After the mixture was sonicated for 10 min, the insoluble [60]fullerene was collected by centrifugation, dried in vacuo, and weighed. The experimental results indicated that 1 mg of **8** (in 1 mL of water) could capture 1.83 mg of [60]fullerene. In the control experiments, it was shown that 1 mg of **6**, which has no L-Try residues, only adsorbed 0.08 mg of [60]fullerene, while gold colloids PPR **2** and **4** displayed no enrichment ability toward [60]fullerene under identical experimental conditions. These solubility experiments were repeated three times, and the errors were found to be <10%. Considering the structural features of aggregate **8**, we deduced that this high [60]fullerene adsorption ability of **8** might arise from the interactions between L-Try residues and [60]fullerene, which was further verified by fluorescence spectral experiments described below. As shown in Figure 11, the emission intensity of an L-Try-CD solution ($5.0 \times 10^{-6}$ mol $dm^{-3}$, 3 mL) was seen to decrease with the addition of PPG2000 (1 $\mu$L, final concentration of PPG2000 in the sample cell = $5.0 \times 10^{-7}$ mol $dm^{-3}$), accompanied by a slight blue shift (from 358 to 354 nm) of the emission peak, which may be attributed to the threading of the PPG chain into CD cavities excluding the L-Try residues. Moreover, the addition of a gold colloid (1 $\mu$L, final concentration of gold colloid in the sample cell = $5.0 \times 10^{-8}$ mol $dm^{-3}$) to the resultant L-Try-CD/PPG mixture further decreased its fluorescence (Figure 11c) due to the quenching effect of Au nanoparticles.[47] Subsequently, 1 mg of [60]fullerene was added to the above-mentioned L-Try-CD/PPG/Au system, and the mixture was stirred for 10 min

(44) Storhoff, J. J.; Lazarides, A. A.; Mucic, R. C.; Mirkin, C. A.; Letsinger, R. L.; Schatz, G. C. *J. Am. Chem. Soc.* **2000**, *122*, 4640−4650.
(45) Braun, M.; Atalick, S.; Guldi, D. M.; Lanig, H.; Brettreich, M.; Burghardt, S.; Hatzimarinaki, M.; Ravanelli, E.; Prato, M.; Eldik, R. V.; Hirsch, A. *Chem.—Eur. J.* **2003**, *9*, 3867−3875.

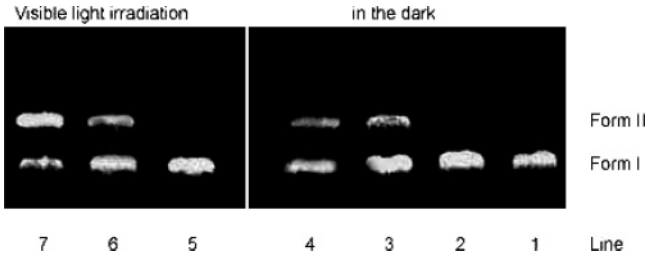


***Figure 12.*** Agarose gel electrophoretic patterns of plasmid DNA. The reaction samples contained 2.0 $\mu$g of pBR322 plasmid. Line 1: no reagent in 50 mM Tris−HCl buffer (pH 7.4). Lines 2 and 5: 2.5 $\mu$g/$\mu$L of PPR **2**. Lines 3 and 6: 2.5 $\mu$g/$\mu$L of **8**. Lines 4 and 7: 2.5 $\mu$g/$\mu$L of **8**−$C_{60}$ system. Lines 1−4: incubated in the dark for 6 h. Lines 5−7: incubated under visible light irradiation at 20 °C for 6 h. Electrophoresis was performed by using 1% agarose gel containing ethidium bromide (0.5 $\mu$g/L).

and then deposited until the solution turned clear. It is worth noting that the fluorescence intensity of the resultant solution was found remarkably quenched, as compared with that of its precursor L-Try-CD/PPG/Au (Figure 11d). This phenomenon indicates that an electron-transfer process from the electron donor Try residues to the electron acceptor $C_{60}$ may have occurred.[44] In control experiments, neither L-Try-CD nor L-Try-CD/Au showed any appreciable fluorescence change with the addition of [60]fullerene under the same conditions. This indicates that the fullerene-capturing ability is a special function of aggregates and does not belong to any of its components. Although this concept has been drawn from a mimic system of Au−PPR aggregates, it should be feasible to extend it more generally to a wide variety of supramolecular assemblies and to explore its future potential applications in the field of material chemistry.

**DNA Cleavage Ability.** We chose a pBR322 plasmid as a substrate to investigate the DNA cleavage ability of the [60]-fullerene-functioned aggregate **8** (Figure 12). In the dark, neither CD-PPG nor L-Try-CD/PPG PPR displayed any DNA cleavage ability. However, aggregate **8** showed a relatively weak DNA cleavage ability both in the presence of light and in the dark (lines 3 and 6). The cleavage mechanism of **8** was probably similar to that of the SbcCD protein with DNA reported by Leach et al.,[48] where the SbcC and SbcD polypeptides in vivo could recognize and cleave DNA.[49] In the present case, due to the presence of numerous L-Try residues, aggregate **8** can also be regarded as a type of pseudopolypeptide, and therefore its DNA cleavage ability seems reasonable. Significantly, after being saturated by [60]fullerene, the **8**−[60]fullerene system exhibited much higher DNA cleavage activity under visible light irradiation (line 7). Most of the closed supercoiled (Form I) DNA was converted into nicked circular (Form II) DNA under light irradiation, which can be attributed to a photoinduced electron transfer from the guanine moiety of DNA to the fullerene via a singlet oxygen transfer.[50]

## Conclusion

A series of Au−PPR aggregates were prepared and comprehensively characterized. The experimental results indicate that amino-terminated PPRs can be adsorbed on the surface of Au nanoparticles through electrostatic interactions between the terminal amino groups and gold particles. The sizes as well as the sedimentation rates of resulting aggregates are enhanced with an increase in the PPR length. Significantly, the polypeptide-like aggregate **8**, possessing numerous L-Try residues, was found to be fairly soluble in water and able to capture and enrich [60]-fullerene. The resultant **8**−fullerene conjugate showed both a satisfactory water solubility and a high DNA cleavage ability under light irradiation and may lead to the potential application of these aggregates in material and biological science.

**Acknowledgment.** We are grateful to the National Natural Science Foundation (90306009 and 20272028), the Tianjin Natural Science Foundation (043604411), and the Ministry of Education of China (20010055001) for financial support. We thank Dr. Xiaopeng Bai and Dr. Hameer Ruparel at Columbia University for their help in the preparation of this article. We also thank the reviewer for his/her highly valuable suggestions regarding the revision.

**Supporting Information Available:** Calculation equations of average surface area occupied by one polypseudorotaxane. This material is available free of charge via the Internet at http://pubs.acs.org.

JA046294W

(46) Sun, Y.-P.; Lawson, G. E.; Huang, W.-J.; Wright, A. G.; Moton, D. K. *Macromolecules* **1999**, *32*, 8747−8752.
(47) Hu. J.; Zhang, J.; Liu, F.; Kittredge, K.; Whitesell, J. K.; Fox, M. A. *J. Am. Chem. Soc.* **2001**, *123*, 1464−1470.
(48) Connelly, J. C.; de Leau, E. S.; Leach, D. R. F. *Nucleic Acids Res.* **1999**, *27*, 1039−1046.
(49) (a) Connelly, J. C.; Leach, D. R. F. *Genes Cells* **1996**, *1*, 285−291. (b) Shurvinton, C. E.; Stahl, M. M.; Stahl, F. *Proc. Natl. Acad. Sci. U.S.A.* **1987**, *84*, 1624−1628.
(50) Ros, T. D.; Prato, M. *Chem. Commun.* **1999**, 663−669.